Degenerate and Non-Degenerate Two-Photon Absorption of Coumarin Dyes

Ismael A. Elayan and Alex Brown*

Department of Chemistry,University of Alberta, Edmonton, Alberta, Canada, T6G 2G2

E-mail: alex.brown@ualberta.ca

Abstract

Two-photon absorption (2PA) spectroscopy is a robust bioimaging tool that depends on the determined cross-sections (σ^{2PA}). The absorption of both photons occurs simultaneously with equivalent (degenerate) or different (non-degenerate) photon energies, D-2PA and ND-2PA, respectively. The former has been investigated experimentally and computationally for many systems, while the latter remains relatively unexplored computationally and limited experimentally. In this study, response theory using time-dependent density functional theory (TD-DFT) and the 2-state model (2SM) have been utilized to investigate $\sigma^{\text{D-2PA}}$ and $\sigma^{\text{ND-2PA}}$ for the excitation to the lowest energy singlet state (S_1) of coumarin, coumarin 6, coumarin 120, coumarin 307, and coumarin 343. Solvents involved were methanol (MeOH), chloroform (ClForm), and dimethylsulfoxide (DMSO), where the latter leads to the largest σ^{2PA}. Values of σ^{2PA} are largest for coumarin 6 and lowest for coumarin, which illustrates the effect of substituents. The 2SM clarifies how the largest cross-sections correspond to molecules with the largest transition dipole moments, μ_{01}. In general, $\sigma^{\text{D-2SM}}$ computations agree with $\sigma^{\text{D-2PA}}$. Moreover, $\sigma^{\text{ND-2SM}}$ are in qualitative agreement with $\sigma^{\text{ND-2PA}}$ with comparable enhancement relative to $\sigma^{\text{D-2PA}}$. Overall, $\sigma^{\text{ND-2PA}}$ are larger than $\sigma^{\text{D-2PA}}$ where the increase is in the range of 22% to 49%. This work aids in future investigations into various fluorophores to understand their photophysical properties for ND-2PA.

Introduction

Coumarin is an aromatic organic compound that is a common fluorescent dye, and it is the parent compound to many derivatives with tuned optical and electronic properties.[1–3] Coumarin, along with its derivatives, are applicable to cell staining,[4,5] useful as fluorescence probes,[6–8] and can act as efficient sensitizers for solar cells.[9–11] However, as fluorescent dyes, their one-photon absorption (1PA) properties are well understood, but there remains questions to be answered for multi-photon absorption in the coumarins.

Photon absorption (PA) is the excitation of a molecule from one electronic state to a higher energy one. In 1931, two-photon absorption (2PA) was first established by Maria Göppert-Mayer,[12] where the absorption of a pair of photons occurs simultaneously with both photons having similar or different energies. After 30 years and with the invention of lasers, the first experimental findings for 2PA were reported for CaF_2:Eu^{2+}.[13] Compared to one photon absorption (1PA), 2PA is a non-linear process where the absorbed energy is quadratically proportional to the incident light intensity. This quadratic dependence leads to deeper sample penetration and better focus, which are critical for clinical imaging.[14] Moreover, 2PA involves excitation with longer wavelengths, which is an attractive feature for biological imaging, as typical one-photon excitations in the UV-vis region then have 2PA wavelengths in the desired optical window for *in vitro* or *in vivo* imaging. These properties permit important technological applications such as high-resolution microscopy,[15,16] non-destructive imaging,[17,18] and spectroscopy.[19,20]

2PA can be degenerate (D-2PA) or non-degenerate (ND-2PA), where the excitation of a fluorophore occurs within the near-infrared region. For D-2PA, both absorbed photons have the same frequency, *i.e.*, same energy (Figure 1). On the other hand, for ND-2PA, the same excitation energy needed for D-2PA can be obtained where the two photons have different frequencies, *i.e.*, different energies. While D-2PA has been investigated for various

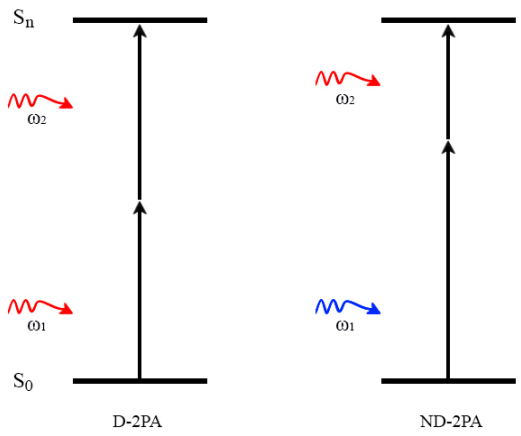

Figure 1: Degenerate ($\omega_1 = \omega_2$) and non-degenerate ($\omega_1 \neq \omega_2$) two-photon absorption. For ND-2PA, ω_1 and ω_2 are the larger and smaller photon frequencies, respectively.

systems,[21–28] ND-2PA remains a somewhat unexplored area. In 1999, the two beams pump-probe measurement approach of the ND-2PA spectra was reported,[29,30] which is based on the use of a strong pump IR beam and a weak probe white light beam.

Attention has been growing recently for determining ND-2PA spectra, the corresponding cross-sections (σ^{2PA}), and the enhancement relative to D-2PA.[31–33] Xue et al.[31] used chloroform as a solvent combined with nanosecond pulses to investigate the D-2PA and ND-2PA spectra of coumarin 6 and coumarin 343; the structures of these coumarins, along with all others considered in the present work are given in Figure 2. On the other hand, Xu et al.[32] used femtosecond pulses and dimethylsulfoxide (DMSO) as a solvent for coumarin 4 and coumarin 120, but the measured σ^{2PA} did not exceed 6 GM (1 GM = 10^{-50} cm^4 s molecule^{-1} photon^{-1}). These small 2PA cross-sections for coumarins are in agreement with the work of Sadegh et al.,[33] which also used femtosecond pulses and DMSO as a solvent to determine the normalized σ^{2PA} for coumarin 343. In general, the measured σ^{2PA} of the coumarin dyes is quantitatively low, but there still remains some discrepancies in the reported values as the results of Xue et al. exceed 45 GM for coumarin 6 and coumarin 343.[31] Differences in measured values for the same coumarins are attributed to the pulse duration, light sources, solvents used, and sample concentration.[21,22,31–33]

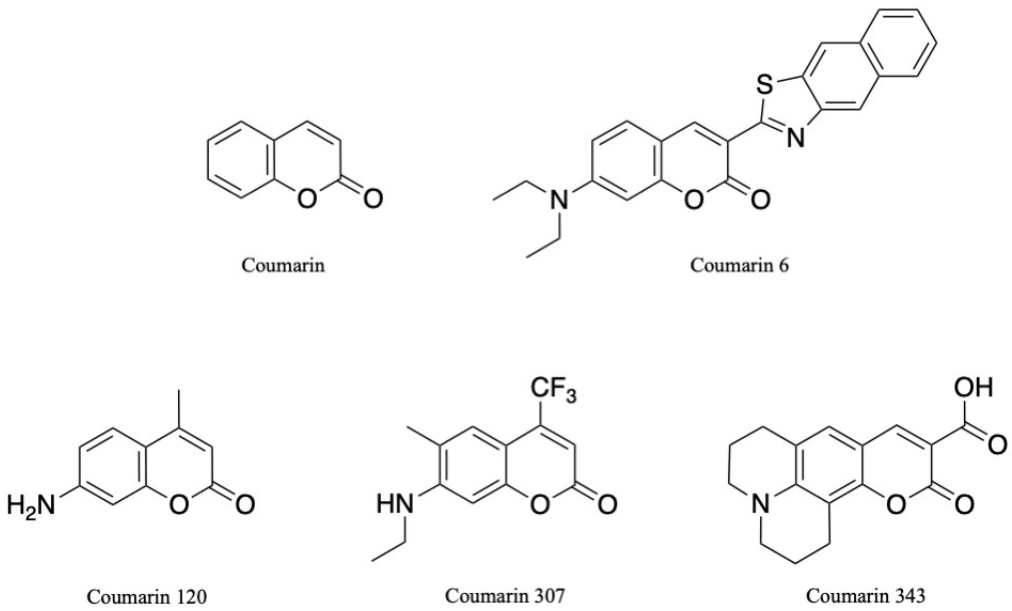

Figure 2: Coumarin fluorophores investigated in this study.

Overall, these studies commonly found that the ND-2PA spectra have similar shapes but different intensities than the corresponding D-2PA spectra. Moreover, the ND-2PA cross-sections, $\sigma^{\text{ND-2PA}}$, have enhanced (larger) values compared to the corresponding D-2PA cross-sections, $\sigma^{\text{D-2PA}}$, where, for example, Sadegh et al. found for coumarin 343 a significant increase of about 40% and up to 75% for fluorescent proteins.[33] The improvements measured in these studies were confirmed theoretically utilizing the essential-state approximation of the sum-over-states (SOS) model. The wide-range of applications of 2PA has resulted in a quest for chromophores with specific desired photophysical properties.[21,34–38] Therefore, understanding the underlying properties governing 2PA in dyes, fluorescent proteins, and small molecules, remains crucial to advance the knowledge of biological imaging as well as for the design of novel imaging agents and advanced dye-sensitizers. In exploring this area, computational chemistry plays a vital role where conclusions drawn provide useful guidelines for the design of efficient dyes.[39–42]

Thus far, the theoretical exploration of ND-2PA has been limited to the SOS model. However, to our knowledge, quadratic response theory has not been applied to understand

measured ND-2PA cross-sections, and these computations will aid in understanding the experimental results. The computational results will also shed more light on the effects of molecular substituents and solvents used on the ND-2PA process. The research utilizes density functional theory (DFT) and time-dependent DFT (TD-DFT) to study the photoexcitation of five common fluorescent coumarin dyes (Figure 2). The previous experimental reported findings will be compared to the 2-state essential SOS model computed herein along with the quadratic response results. Moreover, this work illustrates D-2SM and ND-2SM comparison based on high-level of computations, CAM-B3LYP/aug-cc-pVDZ, relative to computationally predicted cross-sections using response theory, which has not been reported previously. It should be noted that the changes made to difference between ΔE and ω_1, which leads to ω_2, are maintained to not exceed about 0.90 eV, which is adapted from experimental regimes for the reported coumarins.[31,33]

Computational Methods

The geometries of the five coumarins were optimized in methanol (MeOH), chloroform (ClForm), and dimethylsulfoxide (DMSO). The solvent selection was based on the most commonly used solvents in the available experimental studies.[31–33,43–45] The optimization was performed using Gaussian16[46] utilizing Becke's three-parameter exchange hybrid with the Lee-Yang-Parr (LYP) correlation functional in conjunction with the 6-31+G(d,p) basis set.[47,48] Dispersion interactions were accounted for using D3 correction with Becke-Johnson (BJ) damping.[49–52] The computations included the conductor polarizable continuum model (CPCM) where the solvents MeOH, ClForm, and DMSO were used.[53–55] The characterization of the optimized geometry was supported by analysing the computed vibrational frequencies, where the minima structures were determined with no imaginary frequencies.

To study the excitation from the ground state, S_0, to the first singlet excited state, S_1,

TD-DFT,[56] employing quadratic response theory, was used where calculations were performed using Dalton.[57] The long-range corrected B3LYP adopting the Coulomb attenuating method (CAM-B3LYP)[58] has been used with Dunning's correlation consistent, polarized valence, double zeta basis sets, aug-cc-pVDZ.[59,60] The selection of the level of theory was based on a number of benchmarks where CAM-B3LYP was recommended for σ^{2PA} calculations.[27,61–63] Moreover, to use the 2-state model (2SM) approximation for qualitative analysis relative to the quadratic response results, the permanent and transition dipole moments were computed using Gaussian 16 at CAM-B3LYP/aug-cc-pVDZ. Furthermore, all TD-DFT and 2SM calculations were performed using MeOH, ClForm, and DMSO solvents.

In quadratic response theory, the two-photon transition matrix elements, $S_{\alpha\beta}$ where $\alpha, \beta = x, y, z$, and difference between permanent dipole moments between S_0 and S_1 are needed to compute σ^{2PA}. The two-photon transition matrix, $S_{\alpha\beta}$, is expressed as

$$S_{\alpha\beta} = \sum_n \left[\frac{\langle 0|\mu_\alpha|n\rangle \ \langle n|\mu_\beta|f\rangle}{\omega_n - \omega_1} + \frac{\langle 0|\mu_\beta|n\rangle \ \langle n|\mu_\alpha|f\rangle}{\omega_n - \omega_2} \right], \tag{1}$$

where $\mu_{\alpha,\beta}$ corresponds to the Cartesian dipole moment component, ω_n refers to the excitation energy from the initial state $|0\rangle$ to state $|n\rangle$, where f is the final state, which is S_1 herein, and the photon energies are ω_1 and ω_2 ($\omega_1 = \omega_2 = \frac{\omega_n}{2}$ for D-2PA). The 2PA transition moment, δ^{2PA}, is defined as

$$\delta^{\mathrm{2PA}} = \sum_{\alpha\beta} [S_{\alpha\alpha} S^*_{\beta\beta} + 2 S_{\alpha\beta} S^*_{\alpha\beta}]. \tag{2}$$

The cross-section for degenerate 2PA ($\sigma^{\mathrm{D\text{-}2PA}}$) can be computed as

$$\sigma^{\mathrm{D\text{-}2PA}} = \frac{N\pi^2 a_0^5 \alpha \omega^2}{15c\Gamma} \delta^{2PA} \tag{3}$$

where N is set to 4 in single beam, D-2PA, and set to 8 in double beam, ND-2PA,[64] a_0 is

Bohr radius, α is the fine-structure constant, c is the speed of light, and Γ is the lifetime broadening (set at 0.1 eV in the present work). However, for $\sigma^{\text{ND-2PA}}$, the term ω^2 in Equation 3 is $= \omega_1\omega_2$, where ω_1 is the energy of the first photon and ω_2 is the energy of the second photon.

The 2SM is a truncated approximation of the SOS expression (Equation 1) that depends on some physical parameters: excitation energy (ΔE), photon frequency (ω), transition dipole moment (μ_{01}) for the excitation from S_0 to S_1, and permanent dipole moments of S_0 and S_1 (μ_{00} and μ_{11}, respectively). The model provides insight into which physical parameters contribute to the computed σ^{2PA}. In this work, two states are included, the ground state (S_0) and the first excited state (S_1), where in this approximation the cross-sections predicted by the model, σ^{2SM}, are proportional to the square of the difference between the permanent dipole moments from S_0 to S_1, $||\Delta\mu||^2 = (\langle 1|\mu|1\rangle - \langle 0|\mu|0\rangle)^2$, as well as the transition dipole moment, $||\mu_{01}||^2 = \langle 0|\mu|1\rangle^2$. Both cases of degenerate and non-degenerate 2SM cross-sections were computed, corresponding to $\sigma^{\text{D-2SM}}$ and $\sigma^{\text{ND-2SM}}$, respectively. The $\sigma^{\text{D-2SM}}$ was calculated according to Equation 3, while relative change of $\sigma^{\text{ND-2SM}}$ to $\sigma^{\text{D-2SM}}$ (enhancement = Enh.) was computed based on the work of Sadegh et al.,[33]

$$\text{Enh.} = \frac{(\omega_1 + \omega_2)^2}{4\omega_1\omega_2} \tag{4}$$

where ω_1 and ω_2 correspond to the first and second photon energies, respectively.

Results and discussion

The selection of the coumarin dyes is based on the available experimental studies that measure $\sigma^{\text{ND-2PA}}$ or the ND-2PA spectrum relative to the corresponding D-2PA spectrum. Overall, reporting absolute σ^{2PA} is a challenging process and some quantitative discrepancies

are expected when comparing different experimental values or in comparing computationally determined values to experimental measurements. For example, the measured $\sigma^{\text{D-2PA}}$ of coumarin 343 is 48 GM in ClForm (as estimated from the reported experimental spectrum),[31] however, the normalized cross-sections illustrate how far lower it is in DMSO through the reported Enh. results.[33] On the other hand, qualitatively, for a given coumarin, the enhancement of the ND-2PA spectrum (cross-sections), relative to D-2PA is independent of solvent.[31–33] The computed cross-sections of the selected dyes are compared to the available experimental results, quantitatively and qualitatively. By understanding the trends in D-2PA and ND-2AP cross-sections for substituted coumarins, insights into the expected cross-sections enhancements can be obtained and how it can be improved for a variety of interesting fluorophores.

The selected coumarin dyes, see Figure 2, are rigid in structure and the available conformers will have negligible effects on the cross-sections. The main investigation of this work is focused on the computations of ND-2PA cross-sections and their change relative to the corresponding D-2PA ones. As for the solvation effects, the geometry optimization in different solvents shows that there are no observed significant differences between the structures whether in bond lengths or angles, where the determined difference of the former does not exceed 0.005 Å, while for the latter it is 0.001°; it is 3.27° in coumarin 343. This observed angle difference is in the ClForm solvent, which is a result of the rotation of the carboxylic group. However, the solvent selection is maintained in 2PA calculations as the cross-sections are influenced by solvent. The coordinates of the optimized geometries are provided in a separate text file.

Degenerate Two-Photon Absorption

D-2PA computations using quadratic response theory provide ΔE ($\omega_1 + \omega_2$) as well as σ^{2PA}. The computed $\sigma^{\text{D-2PA}}$ in the selected solvents were compared to find the solvent that leads

to the largest values, see Figure 3. The difference in the computed D-2PA cross-sections in the studied solvents for the coumarins does not exceed 9.0%, which is observed in coumarin 343.

The resulting $\sigma^{\text{D-2PA}}$ of the substituted coumarins are much larger than the parent coumarin (Figure 3). For coumarin, $\sigma^{\text{D-2PA}} = 2.02$ GM in DMSO is somewhat larger than the values obtained in MeOH, 1.69 GM, and ClForm, 1.64 GM. On the other hand, coumarin 6 has significant $\sigma^{\text{D-2PA}}$ values of 73.40 GM (DMSO), 63.80 GM (MeOH), and 64.80 GM (ClForm). These large values could be attributed to the electron-donating, $N(Et)_2$, moiety that is substituted at position 7, which aids in the free electronic movement along the π conjugation that is improved by the presence of the aromatic rings on position 2.[65] As for coumarin 120, in DMSO, $\sigma^{\text{D-2PA}} = 23.70$ GM, whereas $\sigma^{\text{D-2PA}}$ in MeOH and ClForm are 19.80 and 20.70 GM, respectively. The obtained values are in agreement with the experimental value $\sigma^{\text{D-2PA}} = 19.30$ GM measured at 754.50 nm (1.64 eV), where ethanol was used as a solvent.[45] Both coumarin 307 and coumarin 343 $\sigma^{\text{D-2PA}}$ values are close in DMSO and MeOH, with differences that do not exceed 3.30 GM. Their cross-sections are in the range

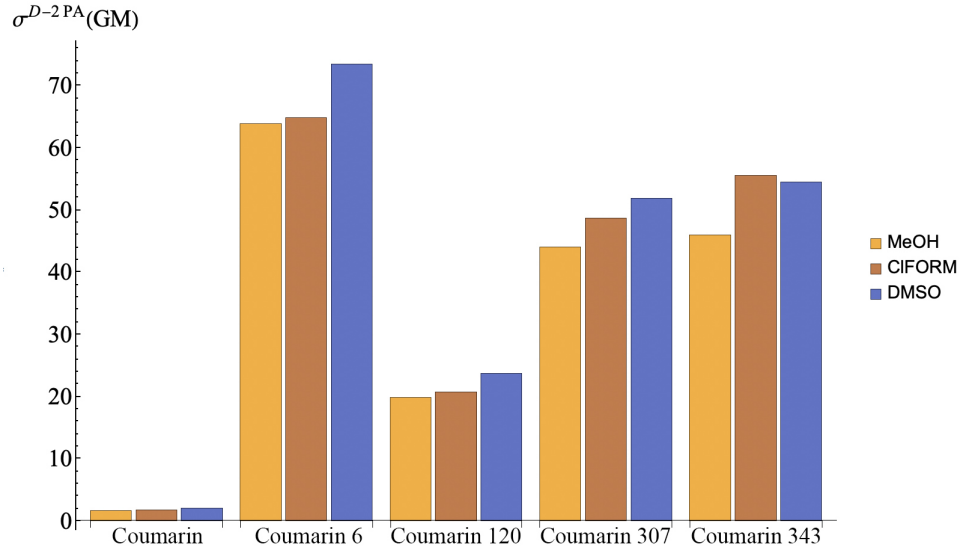

Figure 3: D-2PA cross-sections of the coumarin dyes at CAM-B3LYP/aug-cc-pVDZ in different solvents.

of 44 to 55 GM, larger than coumarin 120 and coumarin, but lower than coumarin 6, which is the one with the highest computed cross-sections. The computed value of $\sigma^{\text{D-2PA}} = 44.00$ GM in MeOH for coumarin 307 is greater than the previously reported value of 16.70 GM at B3LYP/6-31G(d) as well as the experimentally measured value, 19 ± 5.5 GM.[66,67] The difference between the computed values is because of differences in the geometry and level of theory, which affects the computed dipole moments, and thus, cross-sections.[64] In terms of method selection, CAM-B3LYP has been generally recommended for computing 2PA properties for different chemical systems where it was found to produce somewhat closer results to coupled cluster singles and doubles (CC2) and experimental findings.[61–63] Nonetheless, as previously mentioned, σ^{2PA} discrepancies between computational and experimental results are anticipated.

To understand the reasons for the higher cross-sections in DMSO, the transition dipole moments (μ_{01}) for the excitation from S_0 to S_1 have been computed for the used solvents, see Table S1. The results show that MeOH and ClForm give comparable μ_{01} values with the former leading to a somewhat higher magnitude, which reflects on the cross-sections as they are also comparable, as can be seen in the above-mentioned reported data. The highest values are obtained using the DMSO solvent, and thus, it produces the highest computed cross-sections using 2SM and response theory. Therefore, the analysis in the upcoming discussion is based on selecting DMSO as a solvent.

The degenerate 2PA cross-sections predicted using the 2SM, $\sigma^{\text{D-2SM}}$, illustrate the difference between one fluorophore with high $\sigma^{\text{D-2SM}}$ from another with low values, see Table 1. The increase in $\sigma^{\text{D-2SM}}$ values for the dyes is accompanied with larger μ_{01}. Thus, the increase of $\sigma^{\text{D-2SM}}$ and $\sigma^{\text{D-2PA}}$ can be analysed or predicted primarily with the magnitude of μ_{01}. For example, the magnitude, $\mu_{01} = 2.21$ a.u., for coumarin is lower than the other dyes, while for coumarin 6 it is the highest, $\mu_{01} = 4.67$ a.u. This reflects on the evaluated $\sigma^{\text{D-2SM}}$ values where it is lowest for coumarin, 3 GM, and highest for coumarin 6, 71 GM. This is

Table 1: The physical parameters needed for the 2SM for the excitation from S_0 to S_1 in DMSO at the CAM-B3LYP/aug-cc-pVDZ level of theory. Also reported are the cross-sections from the 2SM ($\sigma^{\text{D-2SM}}$) and response theory ($\sigma^{\text{D-2PA}}$).

Dye	ΔE	$\|\|\Delta\mu\|\|$	$\|\|\mu_{01}\|\|$	$\sigma^{\text{D-2SM}}$	$\sigma^{\text{D-2PA}}$
Coumarin	4.33	0.92	2.21	3.25	2.02
Coumarin 6	3.05	1.95	4.67	70.62	73.40
Coumarin 120	3.95	2.06	2.86	28.28	23.70
Coumarin 307	3.46	2.86	3.07	65.70	51.20
Coumarin 343	3.23	2.22	3.98	65.76	54.50

μ in a.u., σ in GM, and ΔE in eV.

in agreement with response theory calculations, *i.e.*, $\sigma^{\text{D-2PA}}$, which is also true for the other dyes. However, slight discrepancies are observed in coumarin 307 and coumarin 343 with differences from response theory of 14.50 and 11.26 GM, respectively. On ther hand, the trend of $\sigma^{\text{D-2SM}}$ is similar to the one predicted by response theory where $\sigma^{\text{D-2PA}}$ for coumarin is lowest and for coumarin 6 is highest, comes after it coumarin 343, coumarin 307, and coumarin 120. Therefore, theoretical predictions using 2SM agree with the response theory computations both quantitatively and qualitatively, which suggests that 2SM can be used for ND-2PA to analyse the cross-sections and the trends therein.

Non-Degenerate Two-Photon Absorption

The approach of doing ND-2PA to compute $\sigma^{\text{ND-2PA}}$ proceeded with changing both ω_1 and ω_2 relative to ΔE with a change of 0.1 eV increment. The investigated systems were scanned based on their individual ΔE, ω_1, and ω_2 values. For example, the 2PA scan of coumarin 6 by changing ω (Figure S1), where first, a D-2PA calculation is performed to find the excited state energy, ΔE = 3.05 eV. Dividing the value of ΔE by a factor of 2 leads to the photon energies, ω_1 and ω_2 = 1.53 eV, with a high $\sigma^{\text{D-2PA}}$ value of 73.40 GM. For ND-2PA, ω_1 is

Table 2: Relative increase in cross-sections from D-2PA to ND-2PA (%) in different solvents (CPCM) at the CAM-B3LYP/aug-cc-pVDZ level of theory. Results are for the largest ω_1 considered for each system.

	Dye				
Solvent	Coumarin	Coumarin 6	Coumarin 120	Coumarin 307	Coumarin 343
MeOH	54.2	20.7	38.8	27.3	20.1
ClForm	43.2	20.5	37.3	24.7	19.2
DMSO	49.5	22.5	41.8	29.6	22.3

changed which is accompanied by a change in ω_2, however, a change from 1.53 eV to 1.63 eV does not result in noticeable changes in the computed $\sigma^{\text{ND-2PA}}$. Thus, such negligible changes are not included in the reported results. As an initial change of $\sigma^{\text{ND-2PA}}$ values, there is a difference of 0.73 GM at $\omega_1 = 1.70$ eV, and it is increasing to 2.15 GM at $\omega_1 = 1.80$ eV. Moreover, increasing ω_1 further to 2.20 eV with a difference of 0.85 eV from ΔE results in $\sigma^{\text{ND-2PA}} = 89.93$ GM. In this system, the difference between ω_1 and ΔE was further scanned to 0.85 eV to illustrate that the difference increases slightly more than the previous photon energies scan and then increases to even a larger difference that leads to extreme ND-2PA with significant enhancement and $\sigma^{\text{ND-2PA}}$ values. The computed $\sigma^{\text{ND-2PA}}$ values are quantitatively higher with a total increase of 22.5%, relative to D-2PA values (Table 2). Similar to D-2PA, coumarin 6 ND-2PA results are largest compared to the other dyes. The resulting improvement of ND-2PA values to D-2PA is in qualitative agreement with the experimental studies.[31–33,68] For a complete overview of $\sigma^{\text{D-2PA}}$ and $\sigma^{\text{ND-2PA}}$, see Figure 4.

Compared to coumarin, coumarin 6 computed cross-sections are larger, however the improvement in coumarin is dramatically higher, 49.5%, where $\sigma^{\text{D-2PA}} = 2.02$ GM at $\omega_1 = 2.17$ eV while $\sigma^{\text{ND-2PA}} = 3.02$ GM at $\omega_1 = 3.30$ eV. In fact, coumarin results in the highest computed improvement investigated, see Table 2. A somewhat comparable $\sigma^{\text{ND-2PA}}$ improvement to coumarin is coumarin 120, where the enhancement is 41.8%, where ω_1 was scanned from

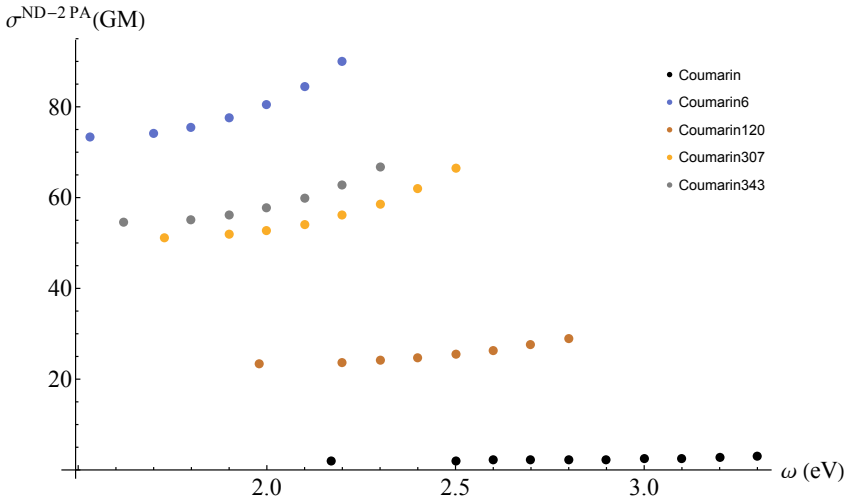

Figure 4: $\sigma^{\text{ND-2PA}}$ as a function of ω_1 ($\omega_2 = \Delta E - \omega_1$) for the studied dyes at the CAM-B3LYP/aug-cc-pVDZ in DMSO level of theory.

1.98 eV, obtained from D-2PA, to 3.00 eV with a corresponding $\sigma^{\text{ND-2PA}}$ value of 33.18 GM. Complete ω scans for the coumarin dyes are provided in Tables S2–S10. Furthermore, coumarin 307 and coumarin 343 are quantitatively close in results, for example see Figures 3 and 4. Particularly at $\omega_1 = 2.5$ eV for coumarin 307, the computed $\sigma^{\text{ND-2PA}} = 66.36$ GM is similar to the value obtained for coumarin 343, $\sigma^{\text{ND-2PA}} = 66.63$ GM at $\omega_1 = 2.3$ eV. Although $\Delta\mu$ and μ_{01} for both dyes are different (Table 1), the cross-sections are similar when the difference between ω_1 and ΔE is lowest. In spite of that, the enhancement computed in coumarin 307 is larger, 29.6%, than coumarin 343 enhancement of 22.3%. It is worth noting that the experimentally measured $\sigma^{\text{ND-2PA}} = 49.00$ GM where $\omega_1 = 1.90$ eV for coumarin 343 in DMSO is comparable to the computed value of 56.23 GM (Table S6).[31]

The 2SM provides enhancement results (Equation 4), which leads to a quantitative measurement of the relative enhancement of the computed cross-sections. The available 2SM results,[31–33] $\sigma^{\text{ND-2SM}}$, have been somewhat limited to low-level computational methods and restricted comparison to experimental studies for the estimated enhancement. For example, ND-2SM applied to substituted fluorene molecules utilized semi-empirical methods to compute the ground and excited state dipole moments, where the model predicts an en-

hancement difference that does not exceed 20% from experimental results.[68] Moreover, the implementation of the model for xanthene, oxazine, coumarin 6, and coumarin 343 dyes to compute 2PA spectra using B3LYP/6-311+G(d) resulted in cross-sections exceeding 250 GM in the calculated spectra, for all species.[31] For coumarin 120,[32] the ND-2PA sum-over-states model with 10 excited states at B3LYP/6-311++G(3df,3pd) shows comparable excitation energies to experiment and reasonable cross-sections agreement within about 50% of experimental measurements. The work of Sadegh et al.[33] showed that for different flourophores the experimentally determined enhancement was higher than the 2SM prediction by no more than 0.53 (Equation 4).

The analysis of $\sigma^{\text{ND-2SM}}$ relative to $\sigma^{\text{D-2SM}}$ depicts the enhancement of ND-2PA cross-sections. For simplicity, the dye with the highest computed cross-sections, coumarin 6, was

Table 3: ND-2PA cross-sections of the 2-state model ($\sigma_\omega^{\text{ND-2SM}}$), ratio of non-degenerate to degenerate photon energies (Enh.) and ND-2PA cross-sections ($\sigma_\omega^{\text{ND-2PA}}$) computed using quadratic response of **coumarin 6** at the CAM-B3LYP/aug-cc-pVDZ level of theory in DMSO.

	Coumarin 6		
ω_1 (eV)	$\sigma_\omega^{\text{ND-2SM}}$	$\sigma_\omega^{\text{ND-2PA}}$	Enh.
1.53†	70.62†	73.40†	1.00
1.7	71.33	74.13	1.01
1.8	72.74	75.55	1.03
1.9	74.86	77.53	1.06
2.0	78.39	80.52	1.11
2.1	82.63	84.54	1.17
2.2	87.57	89.93	1.24
Relative change (%)‡	24.0	22.5	24.0

†D-2PA values.

‡Final σ^{ND} values relative to σ^{D}.

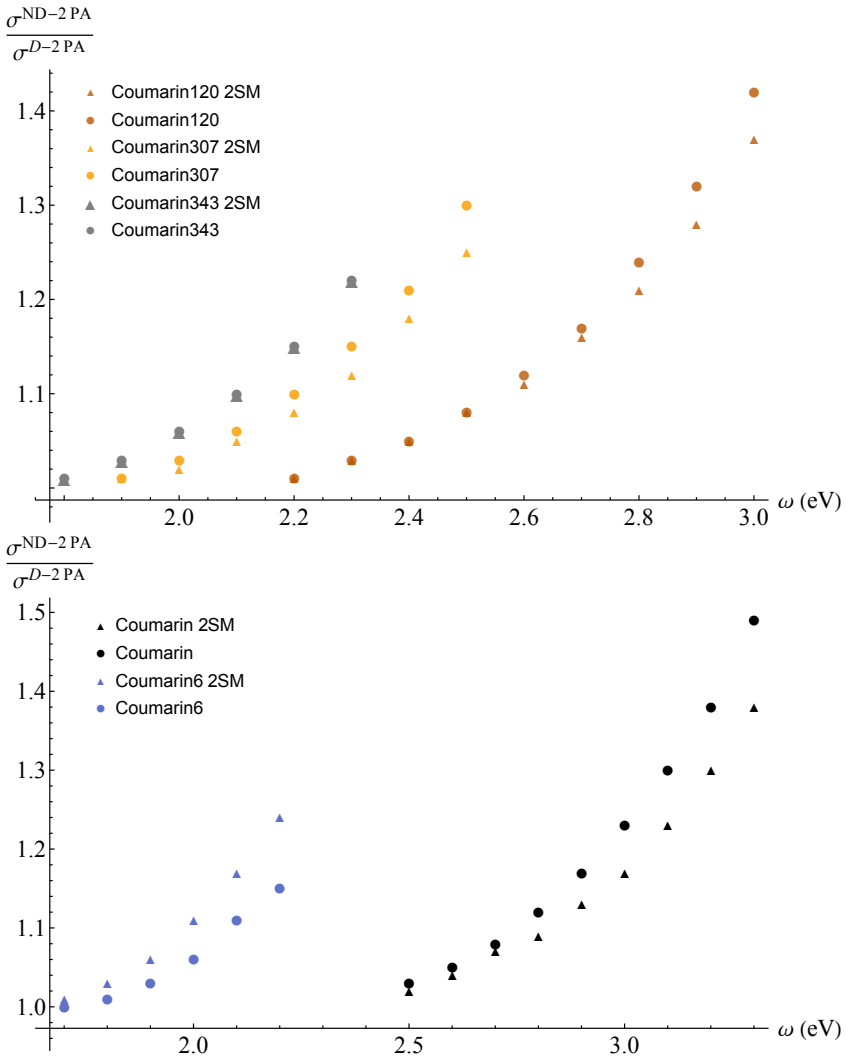

Figure 5: Enhancement results from both response theory and 2SM, as a function of ω_1 ($\omega_2 = \Delta\text{E} - \omega_1$) for the five coumarin dyes, calculated at the CAM-B3LYP/aug-cc-pVDZ level of theory in DMSO.

selected as an example, see Table 3. The predicted $\sigma^{\text{ND-2SM}}$ are relatively in agreement with $\sigma^{\text{ND-2PA}}$. Moreover, the qualitative improvement, 24.0%, is in agreement with the response theory result, within a difference that does not exceed 6.7%. For a full overview of the model comparison to the computed results for the studied dyes, see Figure 5. Interestingly, for coumarin 6, the 2SM predicts that the enhancement is higher than the computed values using response theory, see bottom plot of Figure 5. However, the opposite behavior is observed

for the other coumarin dyes. On the other hand, results of the model are equivalent to the computed response theory results for coumarin 343. For tabulated results of the different dyes, see Tables S7- S10.

In general, ND-2SM is in quantitative as well as qualitative agreement with ND-2PA results. Thus, the considered excitation from S_0 to S_1 for the coumarins is good enough to illustrate the cross-sections and excitation energies. The differences observed are within considerable consistencies to previously reported results that were compared to experimental observations. On a quantitative level, the most observed ND-2SM underestimation is observed in the relative change for coumarin (Table S7), where the difference in the computed relative change between ND-2SM and ND-2PA is 11.3%. Thus, the 2SM approximation suggests that higher-lying excited states might be involved in the cross-sections computations and are necessary to provide better agreement with 2PA results. For the rest of the dyes, it is in agreement with a maximum deviation of 4.6%, which is found in the computed relative change of coumarin 307 (Table S9).

Conclusions

In this study, the computations of ND-2PA cross-sections for five coumarin dyes were reported using response theory and the 2SM approximation utilizing TD-DFT for the transition from S_0 to S_1. Both D-2PA and ND-2PA cross-sections were computed in MeOH, ClForm, and DMSO, where the largest cross-sections were found using DMSO. This increase is (primarily) based on μ_{01} values that were found to be highest in DMSO, relative to the other solvents. To analyse the computed cross-sections using 2SM for D-2PA and ND-2PA, both $\Delta\mu$ and μ_{01} were computed and analysed. The change of ω_1 and ω_2 was based on the difference between ω_1 and the excitation energy of the system, which did not exceed 0.90 eV. Moreover, the work involved comparing the results with D-2PA quantitatively, qualitatively,

as well as the available experimental results.

Quantitatively, the lowest cross-sections are obtained for the parent coumarin dye. However, the substituents were found to increase the computed cross-sections significantly, where the highest values, for D-2PA and ND-2PA, were observed for coumarin 6, then in a descending order, coumarin 343, coumarin 307, and coumarin 120. Moreover, the cross-section analysis using 2SM is in agreement with 2PA results obtained using response theory.

Qualitatively, the cross-sections obtained from ND-2PA are higher than the ones from D-2PA, which is in agreement with the available experimental studies, and this observation is due to enhancement effects. The overall improvement was highest for coumarin (49.5%), then coumarin 120 (41.8%), and coumarin 307 (29.6%), whereas the lowest enhancement obtained was about 22% for coumarin 343 and coumarin 6. The analysis of ND-2SM shows that the enhancement effects increase as ω_1 increases. Interestingly, the 2SM enhancement results are higher than response theory values by 2%, only for coumarin 6, whereas it is lower for the rest of the dyes by at least 6%, and consistent for coumarin 343 by 1.5%.

Acknowledgement

The authors thank the Natural Sciences and Engineering Research Council of Canada (NSERC) for a Discovery Grant to A.B., and Digital Research Alliance of Canada for computing resources.

References

(1) Jacquemin, D.; Perpète, E. A.; Scalmani, G.; Frisch, M. J.; Assfeld, X.; Ciofini, I.; Adamo, C. Time-Dependent Density Functional Theory Investigation of the Absorp-

tion, Fluorescence, and Phosphorescence Spectra of Solvated Coumarins. *J. Chem. Phys.* **2006**, *125*, 164324.

(2) Jacquemin, D.; Perpète, E. A.; Assfeld, X.; Scalmani, G.; Frisch, M. J.; Adamo, C. The Geometries, Absorption and Fluorescence Wavelengths of Solvated Fluorescent Coumarins: A CIS and TD-DFT Comparative Study. *Chem. Phys. Lett.* **2007**, *438*, 208–212.

(3) Dondaine, L.; Escudero, D.; Ali, M.; Richard, P.; Denat, F.; Bettaieb, A.; Le Gendre, P.; Paul, C.; Jacquemin, D.; Goze, C., et al. Coumarin-Phosphine-Based Smart Probes for Tracking Biologically Relevant Metal Complexes: From Theoretical to Biological Investigations. *Eur. J. Inorg. Chem.* **2016**, *2016*, 545–553.

(4) Zhang, W.; Huo, F.; Cheng, F.; Yin, C. Employing an ICT-FRET Integration Platform for the Real-Time Tracking of SO2 Metabolism in Cancer Cells and Tumor Models. *J. Am. Chem. Soc.* **2020**, *142*, 6324–6331.

(5) Niu, H.; Zhang, Y.; Zhao, F.; Mo, S.; Cao, W.; Ye, Y.; Zhao, Y. Reductive Stress Imaging in the Endoplasmic Reticulum by Using Living Cells and Zebrafish. *Chem. Commun.* **2019**, *55*, 9629–9632.

(6) Kong, X.; Li, M.; Dong, B.; Zhang, N.; Song, W.; Lu, Y.; Lin, W. A Near-Infrared and Two-Photon Dual-Mode Fluorescent Probe for the Colorimetric Monitoring of SO_2 in Vitro and in Vivo. *Analyst* **2019**, *144*, 4371–4379.

(7) Yue, Y.; Huo, F.; Ning, P.; Zhang, Y.; Chao, J.; Meng, X.; Yin, C. Dual-Site Fluorescent Probe for Visualizing the Metabolism of Cys in Living Cells. *J. Am. Chem. Soc.* **2017**, *139*, 3181–3185.

(8) Xu, H.; Zhang, H.; Liu, G.; Kong, L.; Zhu, X.; Tian, X.; Zhang, Z.; Zhang, R.; Wu, Z.;

Tian, Y., et al. Coumarin-Based Fluorescent Probes for Super-Resolution and Dynamic Tracking of Lipid Droplets. *Anal. Chem.* **2018**, *91*, 977–982.

(9) Hara, K.; Sato, T.; Katoh, R.; Furube, A.; Ohga, Y.; Shinpo, A.; Suga, S.; Sayama, K.; Sugihara, H.; Arakawa, H. Molecular Design of Coumarin Dyes for Efficient Dye-Sensitized Solar Cells. *J. Phys. Chem. B* **2003**, *107*, 597–606.

(10) Agrawal, A.; Siddiqui, S. A.; Soni, A.; Sharma, G. D. Advancements, Frontiers and Analysis of Metal Oxide Semiconductor, Dye, Electrolyte and Counter Electrode of Dye Sensitized Solar Cell. *Sol. Energy* **2022**, *233*, 378–407.

(11) Chalil Oglou, R.; Ulusoy Ghobadi, T. G.; Ozbay, E.; Karadas, F. "Plug and Play" Photosensitizer–Catalyst Dyads for Water Oxidation. *ACS Appl. Mater. Interfaces* **2022**,

(12) Göppert-Mayer, M. Über Elementarakte Mit Zwei Quantensprüngen. *Ann. Phys.* **1931**, *401*, 273–294.

(13) Kaiser, W.; Garrett, C. Two-Photon Excitation in CaF_2:Eu^{2+}. *Phys. Rev. Lett.* **1961**, *7*, 229.

(14) Denk, W.; Strickler, J. H.; Webb, W. W. Two-Photon Laser Scanning Fluorescence Microscopy. *Science* **1990**, *248*, 73–76.

(15) Denk, W.; Strickler, J. H.; Webb, W. W. Two-Photon Laser Scanning Fluorescence Microscopy. *Science* **1990**, *248*, 73–76.

(16) Xu, C.; Zipfel, W.; Shear, J. B.; Williams, R. M.; Webb, W. W. Multiphoton Fluorescence Excitation: New Spectral Windows for Biological Nonlinear Microscopy. *Proc. Natl. Acad. Sci. U.S.A.* **1996**, *93*, 10763–10768.

(17) Blanchard-Desce, M. Molecular Engineering of NLO-Phores for New NLO Microscopies. *C. R. Phys.* **2002**, *3*, 439–448.

(18) Helmchen, F.; Denk, W. Deep Tissue Two-Photon Microscopy. *Nat. Methods* **2005**, *2*, 932–940.

(19) Rebane, A.; Drobizhev, M.; Makarov, N. S.; Wicks, G.; Wnuk, P.; Stepanenko, Y.; Haley, J. E.; Krein, D. M.; Fore, J. L.; Burke, A. R., et al. Symmetry Breaking in Platinum Acetylide Chromophores studied by Femtosecond Two-Photon Absorption Spectroscopy. *J. Phys. Chem. A* **2014**, *118*, 3749–3759.

(20) Molina, R. S.; Tran, T. M.; Campbell, R. E.; Lambert, G. G.; Salih, A.; Shaner, N. C.; Hughes, T. E.; Drobizhev, M. Blue-shifted Green Fluorescent Protein Homologues are Brighter than Enhanced Green Fluorescent Protein under Two-Photon Excitation. *J. Phys. Chem. Lett.* **2017**, *8*, 2548–2554.

(21) Drobizhev, M.; Makarov, N. S.; Tillo, S. E.; Hughes, T. E.; Rebane, A. Two-Photon Absorption Properties of Fluorescent Proteins. *Nat. Methods* **2011**, *8*, 393–399.

(22) Sánchez-de Armas, R.; San Miguel, M. A.; Oviedo, J.; Sanz, J. F. Coumarin Derivatives for Dye Sensitized Solar Xells: A TD-DFT Study. *Phys. Chem. Chem. Phys.* **2012**, *14*, 225–233.

(23) Li, X.; Rinkevicius, Z.; Ågren, H. Two-photon Absorption of Metal-Assisted Chromophores. *J. Chem. Theory Comput.* **2014**, *10*, 5630–5639.

(24) Salem, M. A.; Brown, A. Two-Photon Absorption in Fluorescent Protein Chromophores: TDDFT and CC2 results. *J. Chem. Theory Comput.* **2014**, *10*, 3260–3269.

(25) Walters, G.; Sutherland, B. R.; Hoogland, S.; Shi, D.; Comin, R.; Sellan, D. P.;

Bakr, O. M.; Sargent, E. H. Two-photon Absorption in Organometallic Bromide Perovskites. *ACS Nano* **2015**, *9*, 9340–9346.

(26) Li, L.; Shang, X.; Wang, S.; Dong, N.; Ji, C.; Chen, X.; Zhao, S.; Wang, J.; Sun, Z.; Hong, M., et al. Bilayered Hybrid Perovskite Ferroelectric with Giant Two-Photon Absorption. *J. Am. Chem. Soc.* **2018**, *140*, 6806–6809.

(27) Rossano-Tapia, M.; Brown, A. Determination of Two-Photon-Absorption Cross Sections Using Time-Dependent Density Functional Theory Tight Binding: Application to Fluorescent Protein Chromophores. *J. Chem. Theory Comput.* **2019**, *15*, 3153–3161.

(28) Zhang, S.; Yang, Z.; Li, M.; Tian, X.; Li, D.; Li, S.; Wu, J.; Tian, Y., et al. A Multi-Photon Fluorescent Probe Based on Quinoline Groups for the Highly Selective and Sensitive Detection of Lipid Droplets. *Analyst* **2020**, *145*, 7941–7945.

(29) Belfield, K. D.; Hagan, D. J.; Van Stryland, E. W.; Schafer, K. J.; Negres, R. A. New Two-Photon Absorbing Fluorene Derivatives: Synthesis and Nonlinear Optical Characterization. *Org. Lett.* **1999**, *1*, 1575–1578.

(30) Negres, R. A.; Van Stryland, E. W.; Hagan, D. J.; Belfield, K. D.; Schafer, K. J.; Przhonska, O. V.; Reinhardt, B. A. Nonlinear Spectrometer for Characterization of Organic and Polymeric Molecules. Organic Nonlinear Optical Materials. 1999; pp 88–97.

(31) Xue, B.; Katan, C.; Bjorgaard, J.; Kobayashi, T. Non-Degenerate Two Photon Absorption Enhancement for Laser Dyes by Precise Lock-in Detection. *AIP Adv.* **2015**, *5*, 127138.

(32) Xu, H.; Chen, S.; Mu, K.; Wang, J.; Tian, Y.; Su, S.; Mao, Y.; Liang, E. Investigation of Nondegenerate Two-Photon Absorption in Common Fluorescent Dyes. *J. Nonlinear Opt. Phys. Mater.* **2018**, *27*, 1850027.

(33) Sadegh, S.; Yang, M.-H.; Ferri, C. G.; Thunemann, M.; Saisan, P. A.; Wei, Z.; Rodriguez, E. A.; Adams, S. R.; Kiliç, K.; Boas, D. A., et al. Efficient Non-Degenerate Two-Photon Excitation for Fluorescence Microscopy. *Opt. Express* **2019**, *27*, 28022–28035.

(34) Marder, S. R. Organic Nonlinear Opt. Mater.: Where we Have Been and Where we are Going. *Chem. Commun.* **2006**, 131–134.

(35) Strehmel, B.; Strehmel, V. Two-Photon physical, organic, and polymer chemistry: theory, techniques, chromophore design, and applications. *Adv. photochem.* **2006**, 111–351.

(36) Terenziani, F.; Katan, C.; Badaeva, E.; Tretiak, S.; Blanchard-Desce, M. Enhanced Two-Photon Absorption of Organic Chromophores: Theoretical and Experimental Assessments. *Adv. Mater.* **2008**, *20*, 4641–4678.

(37) Salem, M. A.; Brown, A. Two-Photon Absorption of Fluorescent Protein Chromophores Incorporating Non-Canonical Amino Acids: TD-DFT Screening and Classical Dynamics. *Phys. Chem. Chem. Phys.* **2015**, *17*, 25563–25571.

(38) Salem, M. A.; Twelves, I.; Brown, A. Prediction of Two-Photon Absorption Enhancement in Red Fluorescent Protein Chromophores Made from Non-Canonical Amino Acids. *Phys. Chem. Chem. Phys.* **2016**, *18*, 24408–24416.

(39) Suseela, Y.; Narayanaswamy, N.; Pratihar, S.; Govindaraju, T. Far-Red Fluorescent Probes for Canonical and Non-Canonical Nucleic Acid Structures: Current Progress and Future Implications. *Chem. Soc. Rev.* **2018**, *47*, 1098–1131.

(40) Pascal, S.; David, S.; Andraud, C.; Maury, O. Near-Infrared Dyes for Two-Photon Absorption in the Short-Wavelength Infrared: Strategies Towards Optical Power Limiting. *Chem. Soc. Rev.* **2021**,

(41) Vuai, S. A.; Khalfan, M. S.; Babu, N. S. DFT and TD-DFT Studies for Optoelectronic Properties of Coumarin Based Donor-π-Acceptor (D-π-A) Dyes: Applications in Dye-Sensitized Solar Cells (DSSCS). *Heliyon* **2021**, *7*, e08339.

(42) Cave, R. J.; Burke, K.; Castner, E. W. Theoretical Investigation of the Ground and Excited states of Coumarin 151 and Coumarin 120. *J. Phys. Chem. A* **2002**, *106*, 9294–9305.

(43) Fleming, G.; Knight, A.; Morris, J.; Morrison, R.; Robinson, G. Picosecond Fluorescence Studies of Xanthene Dyes. *J. Am. Chem. Soc.* **1977**, *99*, 4306–4311.

(44) Rodgers, M. A. Picosecond Fluorescence Studies of Xanthene Dyes in Anionic Micelles in Water and Reverse Micelles in Heptane. *J. Phys. Chem.* **1981**, *85*, 3372–3374.

(45) Fischer, A.; Cremer, C.; Stelzer, E. Fluorescence of Coumarins and Xanthenes After Two-Photon Absorption with a Pulsed Titanium–Sapphire Laser. *Appl. Opt.* **1995**, *34*, 1989–2003.

(46) Frisch, M.; Trucks, G.; Schlegel, H.; Scuseria, G.; Robb, M.; Cheeseman, J.; Scalmani, G.; Barone, V.; Petersson, G.; Nakatsuji, H., et al. Gaussian 16. 2016.

(47) Becke, A. D. Density-Functional Thermochemistry. III. The Role of Exact Exchange. *J. Chem. Phys* **1993**, *98*, 5648–6.

(48) Lee, C.; Yang, W.; Parr, R. G. Development of the Colle-Salvetti Correlation-Energy Formula into a Functional of the Electron Density. *Phys. Rev. B* **1988**, *37*, 785.

(49) Grimme, S.; Antony, J.; Ehrlich, S.; Krieg, H. A Consistent and Accurate Ab Initio Parametrization of Density Functional Dispersion Correction (DFT-D) for the 94 Elements H-Pu. *J. Chem. Phys.* **2010**, *132*, 154104.

(50) Grimme, S.; Ehrlich, S.; Goerigk, L. Effect of the Damping Function in Dispersion Corrected Density Functional Theory. *J. Comput. Chem.* **2011**, *32*, 1456–1465.

(51) Becke, A. D.; Johnson, E. R. A Density-Functional Model of the Dispersion Interaction. *J. Chem. Phys.* **2005**, *123*, 154101.

(52) Johnson, E. R.; Becke, A. D. A Post-Hartree-Fock Model of Intermolecular Interactions: Inclusion of Higher-Order Corrections. *J. Chem. Phys.* **2006**, *124*, 174104.

(53) Cances, E.; Mennucci, B.; Tomasi, J. A New Integral Equation Formalism for the Polarizable Continuum Model: Theoretical Background and Applications to Isotropic and Anisotropic Dielectrics. *J. Chem. Phys.* **1997**, *107*, 3032–3041.

(54) Miertuš, S.; Scrocco, E.; Tomasi, J. Electrostatic Interaction of a Solute with a Continuum. A Direct Utilizaion of Ab Initio Molecular Potentials for the Prevision of Solvent Effects. *Chem. Phys.* **1981**, *55*, 117–129.

(55) Pascual-ahuir, J.-L.; Silla, E.; Tunon, I. GEPOL: An Improved Description of Molecular Surfaces. III. A New Algorithm for the Computation of a Solvent-Excluding Surface. *J. Comput. Chem.* **1994**, *15*, 1127–1138.

(56) Runge, E.; Gross, E. K. Density-Functional Theory for Time-Dependent Systems. *Phys. Rev. Lett.* **1984**, *52*, 997.

(57) Aidas, K.; Angeli, C.; Bak, K. L.; Bakken, V.; Bast, R.; Boman, L.; Christiansen, O.; Cimiraglia, R.; Coriani, S.; Dahle, P., et al. The Dalton Quantum Chemistry Program System. *Wiley Interdiscip. Rev. Comput. Mol. Sci.* **2014**, *4*, 269–284.

(58) Yanai, T.; Tew, D. P.; Handy, N. C. A New Hybrid Exchange–Correlation Functional Using the Coulomb-Attenuating Method (CAM-B3LYP). *Chem. Phys. Lett.* **2004**, *393*, 51–57.

(59) Dunning Jr, T. H. Gaussian Basis Sets for Use in Correlated Molecular Calculations. I. The Atoms Boron through Neon and Hydrogen. *J. Chem. Phys.* **1989**, *90*, 1007–1023.

(60) Woon, D. E.; Dunning Jr, T. H. Gaussian Basis Sets for Use in Correlated Molecular Calculations. V. Core-Valence Basis Sets for Boron through Neon. *J. Chem. Phys.* **1995**, *103*, 4572–4585.

(61) Grabarek, D.; Andruniów, T. Assessment of Functionals for TDDFT Calculations of One-and Two-Photon Absorption Properties of Neutral and Anionic Fluorescent Proteins Chromophores. *J. Chem. Theory Comput.* **2018**, *15*, 490–508.

(62) Beerepoot, M. T.; Alam, M. M.; Bednarska, J.; Bartkowiak, W.; Ruud, K.; Zaleśny, R. Benchmarking the Performance of Exchange-Correlation Functionals for Predicting Two-Photon Absorption Strengths. *J. Chem. Theory Comput.* **2018**, *14*, 3677–3685.

(63) Chołuj, M.; Alam, M. M.; Beerepoot, M. T.; Sitkiewicz, S. P.; Matito, E.; Ruud, K.; Zaleśny, R. Choosing Bad versus Worse: Predictions of Two-Photon-Absorption Strengths Based on Popular Density Functional Approximations. *J. Chem. Theory Comput.* **2022**, *18*, 1046–1060.

(64) Beerepoot, M. T.; Friese, D. H.; List, N. H.; Kongsted, J.; Ruud, K. Benchmarking Two-Photon Absorption Cross Sections: Performance of CC2 and CAM-B3LYP. *Phys. Chem. Chem. Phys.* **2015**, *17*, 19306–19314.

(65) Dudley, C. Chromophore Design for Large Two-Photon Absorption. *Opt. Mater.* **2014**, *37*, 750–755.

(66) Chandra Jha, P.; Wang, Y.; Ågren, H. Two-Photon Absorption Cross-Sections of Reference Dyes: A Critical Examination. *ChemPhysChem* **2008**, *9*, 111–116.

(67) Xu, C.; Webb, W. W. Measurement of Two-Photon Excitation Cross Sections of Molecular Fluorophores with Data from 690 to 1050 nm. *JOSA B* **1996**, *13*, 481–491.

(68) Hales, J. M.; Hagan, D. J.; Van Stryland, E. W.; Schafer, K.; Morales, A.; Belfield, K. D.; Pacher, P.; Kwon, O.; Zojer, E.; Brédas, J.-L. Resonant Enhancement of Two-Photon Absorption in Substituted Fluorene Molecules. *J. Chem. Phys.* **2004**, *121*, 3152–3160.